



Investigation of the non-volatile resistance change in noncentrosymmetric compounds

T. S. Herng^{1*}, A. Kumar^{2*}, C. S. Ong¹, Y. P. Feng³, Y. H. Lu⁴, K. Y. Zeng² & J. Ding¹

¹Department of Materials Science and Engineering, National University of Singapore, 9 Engineering Drive 1, Singapore 117576, Singapore, ²Department of Mechanical Engineering, National University of Singapore, 9 Engineering Drive 1, Singapore 117576, Singapore, ³Department of Physics, National University of Singapore, 2 Science Drive 3, Singapore 117542, Singapore, ⁴Department of Materials Science and Engineering, Zhejiang University, Hangzhou 310027, China.

SUBJECT AREAS:
ELECTRONIC MATERIALS
AND DEVICES
APPLIED PHYSICS
IMAGING
MODELLING AND THEORY

Received
25 June 2012

Accepted
30 July 2012

Published
17 August 2012

Correspondence and
requests for materials
should be addressed to
K.Y.Z. (mpezk@nus.
edu.sg) or J.D.
(msedingj@nus.edu.
sg)

* These authors
contributed equally to
this work.

Coexistence of polarization and resistance-switching characteristics in single compounds has been long inspired scientific and technological interests. Here, we report the non-volatile resistance change in noncentrosymmetric compounds investigated by using defect nanotechnology and contact engineering. Using a noncentrosymmetric material of ZnO as example, we first transformed ZnO into high resistance state. Then ZnO electrical polarization was probed and its domains polarized 180° along the [001]-axis with long-lasting memory effect (>25 hours). Based on our experimental observations, we have developed a vacancy-mediated pseudoferroelectricity model. Our first-principle calculations propose that vacancy defects initiate a spontaneous inverted domains nucleation at grain boundaries, and then they grow in the presence of an electrical field. The propagation of inverted domains follows the scanning tip motion under applied electrical field, leading to the growth of polarized domains over large areas.

On the road towards higher memory density and computer performance, a significant improvement in energy efficiency constitutes the dominant goal in future materials studies. The materials with resistance switching¹ behavior or ferroelectricity² have been widely studied for their nonvolatile memory applications. The resistance switching (Fig. 1b) signifies a dramatic change in resistance under current-limited electrical field modulation¹. The system in low resistance state (LRS) is switched by the threshold voltage into high resistance state (HRS) and vice versa, elucidating the properties of resistance random access memory (RRAM). Many oxide materials, including ZnO³, have shown resistance switching behavior. Possible explanations for the switching behavior include oxygen ion/vacancy migration⁴ and formation/annihilation at the metal/oxide interface⁵, anion migration-induced redox switching¹, phase changes in thin film⁶, and the electron-spin degree of freedom for semiconductor/half metal junctions⁷.

On the other hand, ferroelectricity is a cooperative phenomenon that enables the electrical polarization switching (up/down) under an applied electrical field with a negligible current flow. Interestingly, there are number of materials (e.g. ZnO, GaN, BeO, etc) appear naturally as noncentrosymmetric polar structure. These materials consist of bilayers of alternating positively and negatively charged ions, leading to a spontaneous polarization theoretically^{8,9}. Due to inevitable existence of intrinsic defects and intentional doping, it is essential to take doping effects into consideration when studying spontaneous polarization in such materials. Several experiments have been designed to probe the polarization switching and ferroelectric-like behavior in doped ZnO and GaN^{10–13}. Tagantsev proposed that the ferroelectric-like phenomena in doped ZnO are compatible with Landau model and it is classified as “pseudoferroelectric” or “pseudoferroelectricity”¹⁴. However, the physical origin of the ferroelectric-like behavior in noncentrosymmetric compound is under vociferous debate. One of the rankling obstacles is the insufficient insulating property in these noncentrosymmetric compounds which has hindered the ferroelectric measurement because the applied electric field is screened by conduction electrons. In addition, physical fundamental of polarization switching and/or the formation of inverse ferroelectric domain / domain propagation need to be established.

Tapping into the intriguing properties of polarization and resistance switching in noncentrosymmetric compounds, it is technologically desirable to develop a single material that coexistence of resistance and polarization switching properties. With such materials system, one can probe its polarization switching behavior, when the sample is in the high resistance regime. Here, we demonstrate the hybrid switching (polarization and resistance

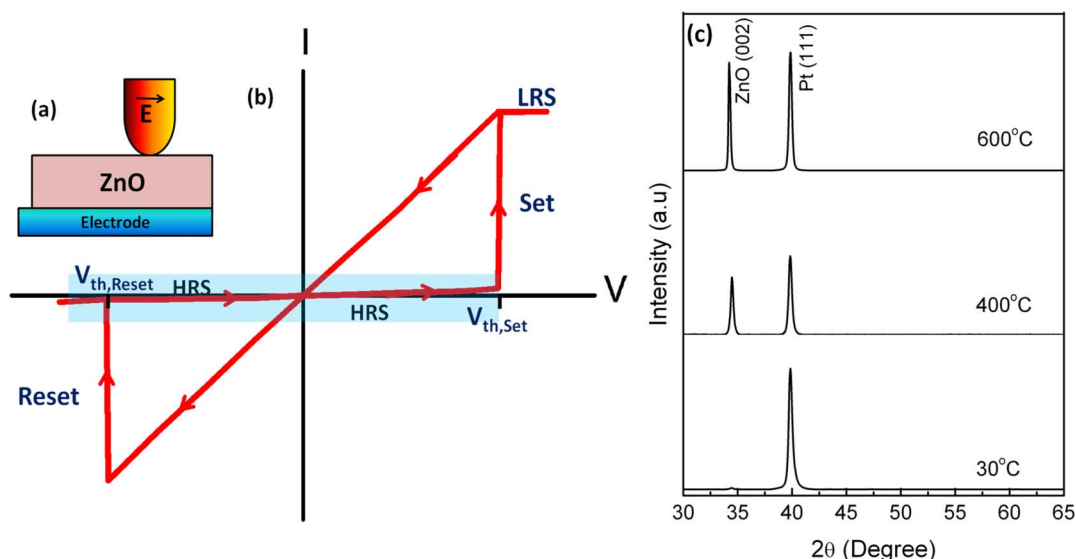


Figure 1 | The conceptual resistance switching of noncentrosymmetric compounds and ZnO structural properties. (a) The schematic diagram of ZnO hybrid switching structure, sandwiched by a top and a bottom electrode. (b) The classical resistance switching characteristic of the ZnO noncentrosymmetric materials. The resistance of noncentrosymmetric materials can be toggled between the low resistance state (LRS) and high resistance state (HRS) via electrical field stimulus. The SET (RESET) operation transform the HRS (LRS) of ZnO into LRS (HRS) when an applied voltage exceeds $V_{th,SET}$ ($V_{th,RESET}$). In the HRS regime, one can apply the electrical field across the sample and the polarization switching behavior can be studied. (c) Temperature dependence x-ray diffraction (XRD) pattern of ZnO on Pt bottom electrode. The ZnO crystallinity improves with an increase of substrate temperature. Pronounced (002) peaks was observed for samples deposited at 400°C and 600°C, respectively. A highly disordered amorphous-like structural of ZnO film was obtained for the samples prepared at the low deposition temperature of 30°C.

switching) characteristic based on noncentrosymmetric compounds. The proposed structure is made of a noncentrosymmetric oxide film (ZnO in our case), sandwiched by a top and a bottom electrode (Fig. 1a). The resistance state of the noncentrosymmetric materials can be toggled between the low resistance state (LRS) and high resistance state (HRS) via electrical field stimulus (Fig. 1b & Fig. 2). Specifically, transformation from the LRS (HRS) to the HRS (LRS) of the noncentrosymmetric oxide film occurs via the SET (RESET) operation, when applied voltage exceeds $V_{th,RESET}$ ($V_{th,SET}$). Once in the HRS regime, one can apply the electrical field across the noncentrosymmetric oxide film and study the polarization switching behavior (Fig. 3). Here by ‘switching’, we refer to the reversal of the dipole moment in the crystal and subsequent retention of the polarization after the electrical field is removed. The ferroelectric-like domains in the noncentrosymmetric crystal can be polarized upward or downward in accordance to the direction of the electrical field.

Among the noncentrosymmetric compounds, zinc oxide (ZnO) has been widely studied for its resistance switching^{15,16} and various switching mechanisms have been proposed^{1,3–7}. Ferroelectric-like^{11–13} characteristics has been reported in doped-ZnO. Furthermore, ZnO is a material of technological importance due to its unique combination of piezoelectric, conductive, and optical properties¹⁷. ZnO is made up of alternative layers of Zn^{2+} and O^{2-} ions stacked in the [001]-direction, forming the Zn–O bilayers (Figs. 4a–c). Each bilayer is stacked on top of another bilayer in the [001]-direction, in the stacking sequence ...AaBbAaBb..., forming a hexagonal close-packed structure. Within each bilayer, there exists a spontaneous polarization due to the net electric dipole moment pointing from O^{2-} to Zn^{2+} . In this work, we demonstrate the non-volatile polarization / resistance switching effect in ZnO via a control of defect nanotechnology and contact engineering (ZnO/Pt). In addition to extensive experimental examinations, modelling and first-principles simulation were carried out to understand the physical origin of ferroelectric-like behaviour in ZnO. Our computational studies indicate that oxygen vacancies (V_O) play a key role in polarization switching. With the assistance of oxygen vacancies (V_O), ferroelectric domain inversion initialises along (110) grain boundary; the polarity

of Zn and O atoms at adjoining position is inverted under an electrical field. More strikingly, these inverted domains can easily spread horizontally (in-plane) over a large area with a low energy barrier along an electrical field direction.

Results

To prove the concept of ZnO based hybrid memory, a series of ZnO films (nominal thickness ~250 nm) was deposited on various bottom electrodes (Pt, Au, ITO, etc) by pulsed laser deposition technique (PLD) at a temperature between 30°C (room temperature) and 600°C under an oxygen partial pressure (P_O) of ~0.2 mTorr (see Methods). All samples exhibit *n*-type semiconductivity with relatively high carrier concentration (see Supplementary Information, Table S1). Figure 1c shows a predominated *c*-axis (002) texture for 400°C and 600°C prepared ZnO films, corresponding to the ZnO wurtzite structure. It is noted that poor crystallinity was observed in films deposited at 30°C. After experimenting with different deposition temperatures and various substrates, we realized that optimum ZnO microstructure can be achieved at deposition temperature between 200°C and 400°C. The Pt substrate provides the better structural and resistance switching properties. The representative samples – ZnO on Pt electrode deposited at 400°C with a thickness of 250 nm were used for a detailed investigation. Figure 2 shows the local resistance switching of ZnO/Pt deposited at 400°C, as determined by conductive atomic force microscopy (C-AFM). The cyclic poling (0 V → 7 V → -8 V → 7 V) was performed on the ZnO film over an area of (5 × 5 μm²) and the corresponding C-AFM images at specific points are displayed in Figs. 2a–g. The average current of each C-AFM image was determined by a commercial software (IGOR Pro 6) and its current density as a function of applied voltage (*J*-*V*) is shown in Fig. 2h. The current starts to ramp up at ~4V and reaches its compliance limit (10 nA) in the range of 5–6 V. Above 6 V, the film possesses high current density with low resistance (LRS). In contrast, the film transforms to the high resistance state (HRS) with negligible current flow after application of -6 V (RESET occurs). We noted that there is a negligible current flow across the film even when a higher voltage of -8 V is applied after RESET

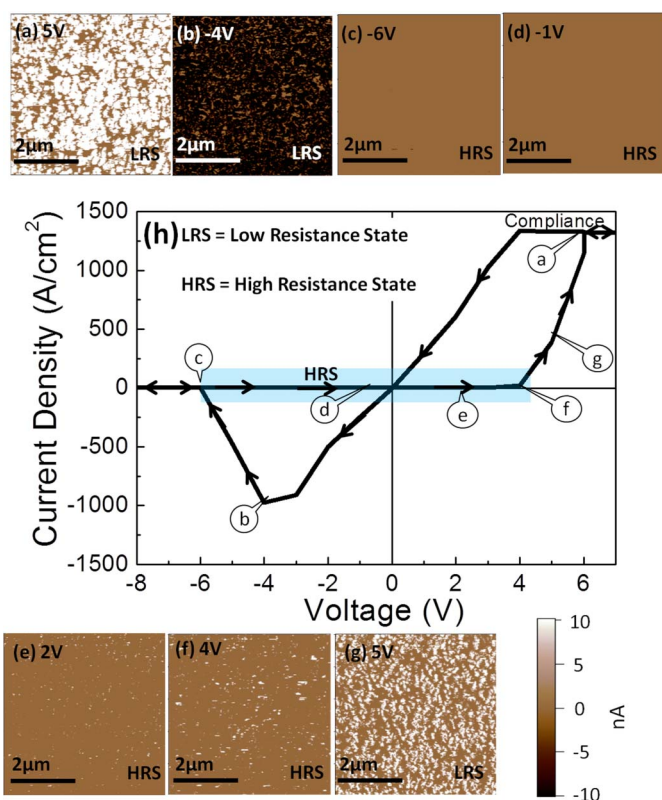


Figure 2 | The resistance switching characteristic of ZnO by conductive atomic force microscope (C-AFM) analysis. (a–g) Using a conducting Pt tip, a cyclic poling (0 V→7 V→8 V→7 V) was performed on ZnO films ($5 \times 5 \mu\text{m}^2$) and C-AFM images were captured. The average current of each C-AFM image was analysed by commercial software (IGOR Pro 6) and its current density is plotted in **h** as function of applied voltage. Apparently, two distinct regimes (LRS and HRS) were observed. Above 6 V, the film possesses high current density with low resistance state (LRS). In contrast, the film transforms to high resistance state (HRS) with negligible current flow after application of -6 V. The film retains its HRS state between -6 V to $+4$ V and this regime is particular important for its polarization switching study. It is noted that voltage is applied to the Pt substrate with tip grounding based on our C-AFM configuration.

operation. This resistance switching phenomenon is repeatable in other regions of the samples as well as other samples (x3). In fact, the observed bipolar resistance switching is consistent with previous experimental results^{3,18}. In the ZnO films being studied, the HRS regime ranged from -8 V to $+4$ V after the RESET operation at -6 V (Fig. 2h). To confirm the Pt tip working condition, the Pt tip condition was checked after each SET→RESET→SET cyclic scanning. The similar 1 V C-AFM images were obtained after each SET operation as compared to its initial 1 V C-AFM image (reference), confirming the Pt tip was in good working mode before and after C-AFM measurement (see Supplementary Information, Fig. S1).

To study the involvement of the polarization switching, piezoresponse force microscope (PFM) measurements were carried out (Fig. 3). It is noted that the electrical field of PFM machine was applied to the tip with respect to substrate grounding, which is opposite to the C-AFM measurement described previously. Conversely, the applied voltage of the C-AFM is applied on substrate with Pt tip grounding. Thus, a positive bias in PFM corresponds to a negative bias in C-AFM and vice versa. To evaluate the effectiveness of HRS regime under PFM setup, we have examined the polarization switching of the ZnO film deposited on Pt electrode at 400°C by PFM system (Fig. 3). Our PFM results have shown that an applied voltage range between $+6$ V and -3 V is sufficient for the polarization switching

investigation with high reproducibility. Therefore, a poling voltage range of $+6$ V and -3 V was used in the PFM experiments and most of PFM discussions below are based on these poling voltages.

Prior to PFM analysis, the ZnO samples were transformed into the HRS regime using the method described above (Fig. 2h). Then using the conductive Pt tip, the high resistive ZnO film was poled by -3 V (Fig. 3a) and $+6$ V (Fig. 3c), respectively over an area of $5.5 \times 5 \mu\text{m}^2$. A remarkable contrast between the unpoled and poled region was observed. The poling results reveal the flipping of domains to upward (downward) direction under the application of a negative (positive) voltage, indicating upward (downward) polarization has been written in the ZnO film. It is also noted that most of the domains were pointing upward at its initial (unpoled) state (see Supplementary Information, Fig. S2b). The corresponding PFM amplitude image (see Supplementary Information, Fig. S2f) depicts volume expansion after negative and positive poling, as supported by amplitude hysteresis loops (see Supplementary Information, Fig. S2g). It is noted that electrical poling has insignificant effect on the surface topography (see Supplementary Information, Fig. S2d), reflecting the film surface is not damaged after poling. More importantly, the polarization in these domains can be manipulated by an electrical field. A remarkable alternative stripes with clear contrast was appeared after a subsequent $+6$ V poling on top of existing -3 V poling pattern (Fig. 3b). The prominent PFM phase contrast difference ($\sim 180^\circ$) between negatively and positively poled regimes is an indication to ZnO pseudoferroelectricity at room temperature. It is worthwhile to highlight that the PFM poling effect is sensitive to its poling conditions (see Method).

To get further insight into the polarization sustainability (retention time), the time dependence PFM imaging was performed. The ZnO film was first poled by $+6$ V, which resulted in a remarkable dark contrast (downward polarization) as shown in Fig. 3c. Then PFM images were taken after 2 hours (see Supplementary Information, Fig. S3c) and 25 hours (Fig. 3d) of poling respectively, both images elucidate the prominent contrast difference between poled and unpoled regimes. Taking PFM images obtained after 2 hours of poling as a reference, statistical results show that more than 90% of polarised domains retained their polarization after 25 hours (see Supplementary Information, Fig. S3e). This long-lasting PFM phase contrast in the high resistive ZnO film excludes the charging effect as a possible origin¹⁹. To further investigate the origin of polarization, the sample was re-scanned after the removal of surface static charge by static-removal device. An insignificant change in PFM phase contrast was found after the surface static charge removal process (see Supplementary Information, Fig. S4). Furthermore, the ground tip scanning experiment was carried out. The polarization of ZnO has been retained after the ground tip scanning across the poled regimes. These observations essentially rule out the role of charging effect in the polarization switching study.

To further probe the polarization switching phenomenon in ZnO, we performed Piezoresponse Force Spectroscopy (PFS) measurement²⁰ (see Methods). Figure 3e shows the voltage dependence of phase hysteresis loop with phase difference of 180° , which is coherent with PFM phase images. A “butterfly shape” piezoresponse amplitude signal was clearly seen in Fig. 3f. It is noted that the amplitude becoming unstable with reduction in its magnitude beyond 6 V and -4 V. Such a phenomenon may be associated to the high current flow in the film that is detrimental to the piezoresponse of ZnO. These PFS hysteresis loops were highly reproducible, as evidenced by our repetitive switching analysis (see Supplementary Information, Fig. S2g and 2h). The concomitant observation of the PFS loops with 180° phase change and “butterfly shape” piezoresponse signals in the high resistive ZnO films attest their polarization switching and pseudoferroelectricity character at room temperature.

Furthermore, we have studied the polarization switching of the ZnO samples deposited at various temperatures. The thickness of

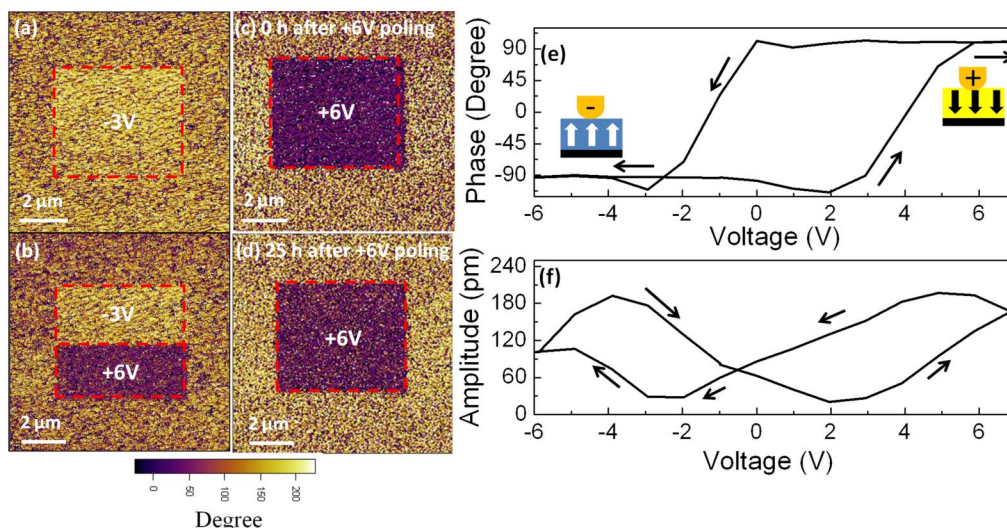


Figure 3 | Direct evidence of polarization switching and pseudoferroelectric properties of ZnO on Pt electrode. Using a conducting Pt tip, the polarization switching of ZnO is studied by PFM technique. (a) The PFM phase images of ZnO ($10 \times 10 \mu\text{m}^2$) after application -3 V over region of $5.5 \times 5 \mu\text{m}^2$ (red dotted regime). (b) A remarkable alternating stripes ($5.5 \times 2.5 \mu\text{m}^2$) is seen after subsequent $+6$ V poling on top of the existing -3 V poling pattern, elucidating the 180° phase change and it is supported by (e) PFM phase hysteresis loop. The corresponding piezoresponse signal of ZnO shown in f depicts the “butterfly shape”. It is noted that the amplitude loop getting unstable with reduction in magnitude above 6 V and -4 V. (c,d) The polarization retention time study, showing majority of polarization are retained after 25 hours. It is noted that voltage is applied to tip with substrate grounding based on our PFM configuration.

ZnO was kept constant at 250 nm. It was found that ZnO deposited at 400°C on Pt electrode exhibited a uniform and stable polarization switching (see Supplementary Information, Fig. S5b). In stark contrast, the ZnO film deposited at room temperature (30°C) shows a very poor electric poling response (see Supplementary Information, Fig. S5a). Similarly, the sample deposited at the higher temperature of 600°C does not show a uniform polarization switching (see Supplementary Information, Fig. S5c). The corresponding enlarged view shows that most dark areas (polarized areas) are concentrated along grain boundaries (see Supplementary Information, insert of Fig. S5c). Figure S6a (see Supplementary Information) shows the statistical distribution of polarized area (see Method) of ZnO film deposited at various temperature, as poled by $+6$ V over region of $5 \mu\text{m}^2$. Three distinct polarization regimes were identified. Apparently, ZnO films deposited at 200 , 300 and 400°C (Regime II) exhibit the strongest polarization with $>90\%$ polarizable domains (see Supplementary Information, Fig. S6a). It is noted that these films were well-crystallized with a (002) texture (Fig. 1c) and grain sizes around 50 nm, as seen by transmission electron microscopy (TEM) analysis. In contrast, weak polarization was detected in the samples deposited at lower temperature (30°C to 100°C ; Regime I) and higher temperature (500°C to 600°C ; Regime III).

To have a clearer picture, we examined the resistivity switching and micro-structural properties of ZnO deposited at 30°C and 600°C , respectively. The ZnO samples deposited at 30°C do not exhibit a high resistance state (HRS) (see Supplementary Information, Fig. S7a) due to high current leakage at high voltage regime. The nature of low resistance and high electron concentration ($8 \times 10^{19} \text{cm}^{-3}$) of 30°C prepared ZnO (see Supplementary Information, Table S1) suppressed the effectiveness of an electric field applies onto the samples, leading to weak pseudoferroelectricity. The microstructure analysis of 30°C prepared film by TEM reveals an amorphous with highly disordered structure (see Supplementary Information, Fig. S6b), which is consistent with our XRD data (Fig. 1c).

On the other hand, the ZnO deposited at 600°C possesses a reasonably good high resistance state (HRS) after the RESET operation of -5 V in negative voltage regime (see Supplementary Information,

Fig. S7b). However, the HRS characteristic failed to expand into the positive voltage regime. A relatively large leakage current was observed when applied voltage exceeded $+1$ V. We noted that these samples exhibited superior structural properties with larger grain size (150 nm to 200 nm) and sharp interface between neighboring grains (see Supplementary Information, Fig. S6c). To further examine its microstructure, we performed the AFM and C-AFM imaging of 600°C prepared ZnO films. By proper reconstructing the AFM and C-AFM images (see Supplementary Information, Fig. S7c & d), we found that the film was rather leaky and most of current leaking areas (white areas) were located near the grain boundaries. Such leaky phenomenon lead to incomplete and weak polarization for the 600°C prepared ZnO samples. This is because parts of grain boundaries do not respond to the applied electrical field due to the electron screening effect. These results seems to imply that large grain size is not favorable for polarization switching in ZnO whereas a nanocrystalline structure (~ 50 nm for 400°C prepared samples) is desirable for pseudoferroelectricity in ZnO.

Moreover, we have studied the thickness dependence pseudoferroelectricity of ZnO, down to 15 nm. All the films were deposited at 400°C . The thinner films were found to exhibit higher percentage of switchable domains (see Supplementary Information, Fig. S11a). In particular, the ZnO films with 15 nm and 30 nm thick have nearly 100% of the polarizable domains. The polarization of thicker films (> 500 nm) with larger grain size (> 100 nm) displayed weakened pseudoferroelectricity. These results further confirm the importance of nanocrystalline structure in the realization of ZnO pseudoferroelectricity.

Since polarization switching is impossible in perfect ZnO crystal (see Supplementary Information, Section B and Fig. S9), defects are expected to play a critical role in polarization switching and pseudoferroelectricity. Native defects such as oxygen vacancies (V_{O}) are commonly observed in *n*-type ZnO. The presence of V_{O} in our films is further supported by the appearance of broad $E_1(\text{LO})$ peak ($\sim 587 \text{cm}^{-1}$) in the Raman spectrum and detection of green emission (centred at ~ 500 nm) in photoluminescence analysis (see Supplementary Information, Fig. S8).

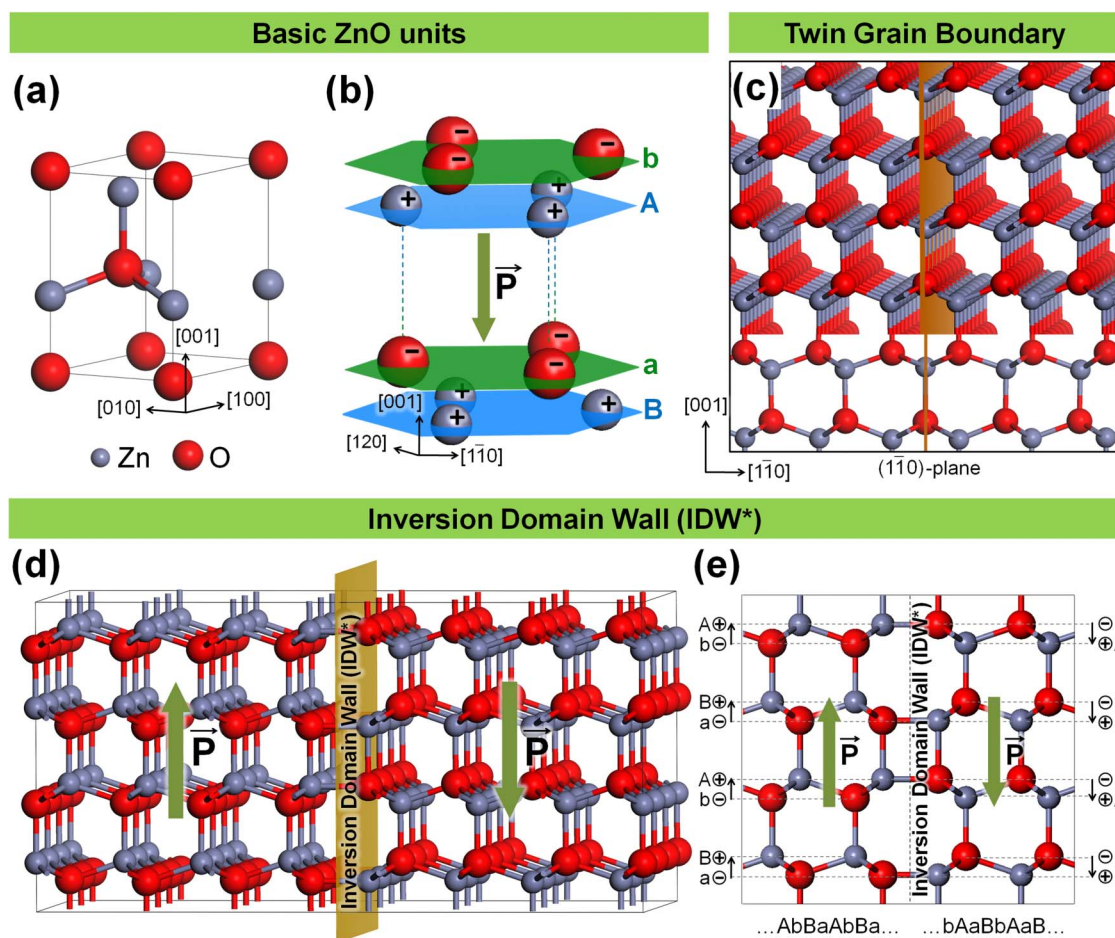


Figure 4 | The atomistic model of wurtzite ZnO, a twin grain boundary and an inversion domain wall (IDW*). (a) ZnO unit cell, including the tetrahedral-coordination between Zn and its neighboring O. (b) ZnO has a noncentrosymmetric crystal structure that is made up of alternate layers of positive and negative ions, leading to spontaneous polarization \vec{P} . The pseudoferroelectric switching involves the reversal of these dipole moments. (c) A low-energy twin ($1\bar{1}0$) boundary that was used to model the grain boundary. (d) A 3D representation of the domain wall in the ($1\bar{1}0$) plane, separating two oppositely-polarised ZnO domains. (e) The corresponding 2D representation of **d**.

To understand the underlying mechanism of polarization switching in ZnO, we carried out first-principles simulation. It is recalled that our experimental results have shown the importance of the nanocrystalline structure and V_{O} towards ZnO pseudoferroelectricity. In addition, the results suggest that polarization switching is initiated at grain boundaries. Taking all experimental observations into consideration, we performed extensive modeling and first-principles calculations based on the Density Functional Theory (DFT) as implemented in the Vienna *ab-initio* simulation package (VASP) (See Methods). Accordance to our experimental observations that ZnO possesses a predominant (002) texture and most of the domain walls are perpendicular to the film, thus we modeled the domain wall with the ($1\bar{1}0$) plane. It is perpendicular to the (002) plane and is commonly present in ZnO system^{21,22}. The ($1\bar{1}0$) is also known as the m-plane for wurtzite ZnO and is symmetrically equivalent to and representative of a family of domain boundaries, including ($\bar{1}10$), (010), (100), (0 $\bar{1}0$) and ($\bar{1}00$)^{22,23}.

Specifically, a twin boundary (Fig. 4c) was used to model the grain boundary structure as it was found to have a low formation energy of 0.06 eV/Å². The formation energy of an oxygen vacancy (V_{O}) at the grain boundary was first evaluated and compared to that in bulk ZnO. The results signify a thermodynamic preference of oxygen vacancy to form at the grain boundary because its formation energy at the grain boundary is always lower than that in bulk by about 0.44 eV (see Supplementary Information, Fig. S10). Subsequently,

we carried out modeling and calculations to investigate the pseudoferroelectricity in ZnO in three key steps. First, a three-dimensional (3D) ZnO inversion domain model was developed and evaluated. Second, the switching mechanism of inverted domains along the ($1\bar{1}0$) boundary was studied. Finally, the propagation of ZnO pseudoferroelectric domains over large areas via domain wall movement was evaluated.

ZnO unit cell possesses a spontaneous electric dipole moment and its orientation is along the [001]-direction as shown in Fig. 4b. Certainly, such an electric dipole moment is not the same as that in typical ferroelectric materials, such as BaTiO₃, in which polarization switching is realized by the movement of the smaller Ti cations about off-center position²³. Therefore, the ferroelectric-like behaviour found in ZnO is termed as “pseudoferroelectricity”. Our experimental results showed that the ZnO film is highly textured in the predominant [001]-direction (Fig. 1c) and a scanning PFM tip can polarize ZnO upwards in the [001]-direction or downwards in the [00 $\bar{1}$]-direction. ZnO can thus be said to adopt either of the two orientational states (Fig. 4d): upwards or downwards. In between two oppositely polarized domains, an inversion domain wall (IDW*) exists and its structure has been previously proposed^{21,24}. Our calculation confirms that an inversion domain wall as shown in Fig. 4d has a formation energy of 0.01 eV/Å². Figures 4d and 4e mark out the ZnO dipole moments polarized upwards in the [001]-direction and downwards in the [00 $\bar{1}$]-direction and separated by an inversion domain wall (IDW*).

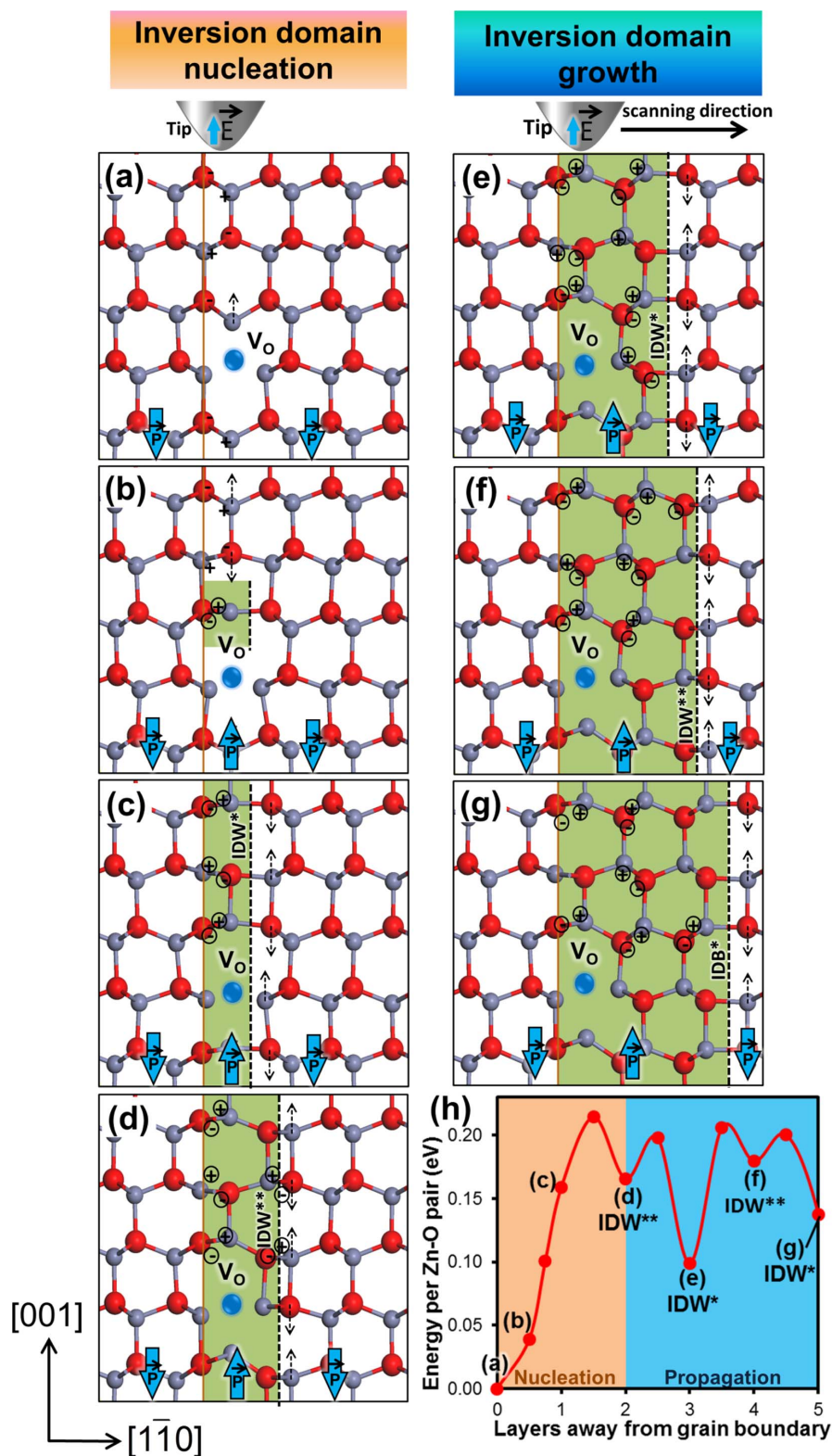


Figure 5 | Outline of pseudoferroelectric domain nucleation, propagation and growth. (a–d) Nucleation of a pseudoferroelectric domain at a ZnO ($1\bar{1}0$) boundary. (a) Due to the presence of the V_o , the Zn atom above lost its bonding to the missing oxygen. (b) Under an electric field, the positively charged Zn ion moves up in the vertical direction (c), the polarity of Zn and O atoms at the adjoining position is then inverted and the inversion spreads vertically along the boundary rapidly, leaving a trail of inversion ferroelectric domain in its wake and forming an inversion domain wall (IDW*) along the grain boundary. (d) In the presence of an external electric field, Zn^{2+} and O^{2-} at the IDW* experience an electric force and are displaced in opposite directions by 0.5\AA , relieving the strain in its four-membered ring forming an IDW**. (e–g) The propagation of pseudoferroelectric domain wall from left to right in the presence of an external electric field. (e) An electric force on Zn^{2+} and O^{2-} at the IDW** once again displaces Zn^{2+} and O^{2-} in opposite directions by about 0.5\AA , regenerating an IDW*. (e–g) Propagation of the inversion domains wall in the sequence $\dots IDW^* \rightarrow IDW^{**} \rightarrow IDW^* \dots$ (h) Energy profile of the nucleation and propagation of the pseudoferroelectric domain. The dotted arrows represent the displacement direction of Zn and O atoms under application of electrical field.



Similar to classic ferroelectric materials, one can expect the polarization switching in ZnO to be initiated by the formation of the very first inverse domain wall followed by the spreading of the inversion domain to complete the depolarization via domain wall propagation. Thus, we have performed a careful study on the formation of an inverse pseudoferroelectric domain. It is found that inverse domain cannot be formed in perfect ZnO crystal because the energy barrier of ion diffusion is too high (over 5 eV per Zn-O pair). The details ZnO pseudoferroelectric evaluation are available in Section B of Supplementary Information, Fig. S9. Therefore, we considered a more realistic scenario – the polarization in ZnO is assisted by V_O defects as V_O is abundant in the ZnO samples, as evidenced by Raman, PL and Hall-effect measurements.

Since our first-principles calculations indicated that V_O is more likely to form at grain boundaries (see Supplementary Information, Fig. S10), we developed a model that involves the nucleation of an inversion domain along the grain boundary assisted by V_O . Figures 5a–d show a schematic representation of the nucleation process of a pseudoferroelectric domain which is induced by V_O at the (110) boundary. Due to the presence of the V_O , the Zn atom above lost its bonding to the missing oxygen (Fig. 5a). Under the applied electric field, the positively charged Zn ion moves up in the vertical direction (Fig. 5b). The polarity of Zn and O atoms at adjoining position is then inverted and the inversion spreads vertically along the boundary rapidly, leaving a trail of inverted pseudoferroelectric domain in its wake and forming an inversion domain wall (IDW*) along the grain boundary (Fig. 5c).

Next, we will evaluate the propagation of inversion domains wall over large area. Once an inversion domain is formed, it can propagate easily and laterally in the direction of the scanning tip under the presence of electrical field. Due to the external electric field applied in the [001]-direction, Zn^{2+} and O^{2-} at the inversion domain wall (IDW*) experience an electric force (Fig. 5c) and are displaced in opposite directions by about 0.5 Å in response to the applied field (Fig. 5d). This relieves the strain in its four-membered ring while forming another four-membered ring at a new boundary structure, denoted here as IDW** (Fig. 5d). IDW** is structurally similar to IDW*, except for the minor displacement of Zn-O pairs as described above. Upon formation of this new intermediate boundary structure IDW**, the domain wall has propagated in that same direction (IDW* → IDW**) (Fig. 5c → Fig. 5d). In the energy profile (Fig. 5h), we see that this configuration corresponds to a local energy minimum. The nucleation of inversion domain under an applied electrical field has a low energy barrier of ~0.2 eV per Zn-O pair.

Sustained application of an electric field in the scanning direction then causes the inversion domain wall to propagate. Zn^{2+} and O^{2-} at the IDW** experience an electric force (Fig. 5d), once again displacing Zn^{2+} and O^{2-} in opposite directions by about 0.5 Å (Fig. 5e). This similarly relieves the strain in the 4-membered ring at the IDW** and re-forms an IDW* in the propagation direction (IDW** → IDW*) (Fig. 5d → Fig. 5e), driving the propagation further. Subsequently, the inversion domains wall propagates continuously in the sequence ... IDW* → IDW** → IDW* ... (Fig. 5e → Fig. 5g), which is facilitated by the cyclic relief of strain in four-membered rings. In response to the electric field, the pseudoferroelectric domain is polarized in the direction parallel to the applied field and grows in size. As the PFM tip scans across the (001)-plane, the domain wall propagates continuously, switching electric dipoles along the way, until it meets another wall. Two neighboring pseudoferroelectric domains then coalesce to form one larger domain. As shown in Fig. 5h, the largest propagation barrier is only ~0.1 eV per Zn-O pair.

Discussion

As discussed above, our experimental results indicate that grain size plays an important role in ZnO pseudoferroelectricity. Smaller grain

size enables an effective polarization switching, while larger grain size is accompanied by a partial polarization switching with a significant leakage current (see Supplementary Information, Fig. S7b). Analogy to the concept of single domain particle size in ferromagnetic materials²⁴, we could obtain the value around 25 nm for “single domain pseudoferroelectric ZnO particle” based on the minimization of domain wall energy and dielectric field energy. This theoretical grain size is closer to the experimental grain size (~50 nm) of ZnO film that prepared at a temperature range of 200–400°C. The formation ability of domain wall with grain size is also estimated based on 1st principle calculations. It is found that domain wall could occur spontaneously at room temperature in the grain with size larger than 25 nm. The density-of-state (DOS) of ZnO with a domain wall structures suggest that domain walls have a high conductivity (metal-like transport properties), as the Fermi level lies in the conduction band. That explain why large grain size is not favourable for polarization switching due to spontaneously formation of conductive domain wall. It is in agreement with the experiment observations that current leakage is located near the grain boundary (see Supplementary Information, Fig. S7d). In fact, our result is consistent with the classic ferroelectric materials that possess higher conductivity in the domain wall²⁵. The domain wall conductivity in a ferroelectric materials has been shown via numerical calculation previously²⁶. Such conductive domains wall leads to weakened pseudoferroelectricity in the ZnO sample with a larger grain size.

In conclusion, we have demonstrated room temperature non-volatile polarization and resistance switching in ZnO via a deterministic control of the oxygen vacancies, carrier concentration, nano-grain structure, grain boundaries and contact engineering. The pronounced resistance switching behaviors (low resistance state (LRS) ↔ high resistance state (HRS)) was observed in ZnO films prepared at 400°C with its average grains size of 50 nm. In the HRS regime, ZnO domains can be polarized with 180° phase switching along the [001] axis by an electrical field. The polarization was long-lasting (more than 25 hours) and ferroelectric domains could be written and erased repetitively. An oxygen vacancy (V_O) mediated pseudoferroelectricity model is proposed to explain satisfactorily the nucleation and propagation of inversed domain. Based on this model, polarization switching initiates at the inversion domain boundaries (IDW*) in the presence of V_O , such that the Zn-O polarity is inverted along the (110) boundary under an applied electric field. The nucleation of inversion domain under an applied electrical field has a low energy barrier of ~0.2 eV per Zn-O pair. With a mutual complement of the spontaneous domains nucleation and propagation, Zn^{2+} and O^{2-} ionic pair with an energy barrier of 0.1 eV will migrate and switch along the direction of the applied electric field, leading to the growth of inverted domains over a large area. This accomplishment offers exciting opportunities for the fabrication of ZnO multiple bits information storage that is compatible with today's silicon technology.

Methods

Films preparation and characterizations. ZnO powders (99.99%, Sigma-Aldrich) are used in the present study to make an undoped ZnO pallet, then it was sintered at 1000°C for 12 hours to obtain ZnO target. We have carried out an extensive parameters optimization to obtain superior crystalline ZnO films with a prominent *c*-axis (002) texture (Fig. 1c). With these optimum conditions, a series of ZnO films with a nominal thickness of 250 nm was prepared on Pt bottom electrode by pulsed laser deposition (PLD) using a KrF excimer laser operating at 248 nm and a fluence of 1.8 J cm⁻², ranging from room temperature (30°C) to 600°C under oxygen partial pressure of 0.2 mTorr. Our study shows that ZnO crystallinity and structural properties are sensitive to deposition temperature. The low temperature (<200°C) deposited ZnO films possessed the amorphous-like structure. To have an in-depth understanding of ZnO ferroelectricity, we carried out the thickness dependence study. A series of ZnO film with various thicknesses was deposited on the platinum (Pt) bottom electrode (ZnO deposited on Pt/Ti/Si/SiO₂ substrate) under oxygen partial pressure of 0.2 mTorr at 400°C, ranging from 15 nm to 600 nm. The structural properties improved with an increase film thickness, but degradation in pseudoferroelectricity. To obtain uniform oxygen distribution across the films, the samples were kept at identical deposition temperature and oxygen partial pressure for



~30 mins prior to cooling down. Then the samples were slowly cooled down to room temperature under oxygen ambient (partial pressure ~0.2 mtorr). It is worthwhile to highlight that all the samples were sealed by parafilm immediately after the deposition and kept in a dry box, in order to avoid oxidation.

The structural properties of the samples were studied by X-ray diffraction (XRD; Bruker AXS D8 Advance), TEM (Joel, JEM 2010F) and Raman spectroscopy (LabRam HR 800). The green emission was analyzed by the integrated photoluminescence system (JY-Horiba, FluoroLog-3 spectrofluorometer) under excitation of 325 nm He-Cd laser source (30 mW).

Resistance switching analysis. The local resistance switching behaviors were investigated by conductive atomic force microscope (Asylum Research), using a commercially available Pt-coated tips. Conductive Pt tips (AC240TM Olympus, Japan) with 15 nm tip radius, 2 N/m stiffness and its resonance frequency of 70 kHz was used. The commercial software (IGOR PRO 6.12A) together with the Asylum Research code (version 090909-1214) was used to get the average current distribution of C-AFM image. An average current density as function of voltage is plotted.

Pseudoferroelectric properties. A commercial vertical Piezoresponse force microscopy (VPFM, MFP-3D, Asylum Research, USA) is used to characterize the ferroelectric and local switching behaviours of ZnO film. Conductive tips (AC240TM, Electric-Lever, Olympus, Japan) with 15 nm tip radius, 2 N/m stiffness and its resonance frequency of 70 kHz was used. It is worthwhile to highlight that the poling process is sensitive to scan speed, poling voltage, and the contact between the tip and ZnO film. Thus, extensive optimizations have been performed to get the reliable and best PFM images. For the dc poling, a line scanning method with a scanning speed of 12.5 $\mu\text{m/s}$, response drive amplitude of 1 V, set point of 0.6 V and frequency of 1 Hz frequency was employed. Furthermore, poling effect is depended on the tip Pt coating quality. The Pt tip with a resonant frequency ~70 kHz and work function difference of ~500 mV (between ZnO and Pt tips, as determined by Kelvin Probe Force Microscopy (KPFM) technique) always offers good poling results. It is also noted that samples oxidation may affect the PFM analysis, thus all the samples were sealed and kept in the dry box immediately after the deposition.

In Piezoresponse Force Spectroscopy (PFS)²⁰ investigation, a sine-like triangular waveform that carried a sequence of square waves with its frequency of 400 mHz was applied to the tip. The remnant bias-induced polarization is acquired at every pulse between the adjacent voltage steps when the bias is stepped back to zero.

The commercial software (IGOR PRO 6.12A) together with the Asylum Research code (version 090909-1214) was used to get the statistical distribution of switched domains. This operating system captures the PFM scanned information (such as piezoresponse, polarization, etc.) of each pixel. This information can be further used for the statistic distribution calculation.

First-principles calculation and modeling. To model the ferroelectric phase transition, we carry out first-principles calculations based on the Density Functional Theory (DFT) as implemented in the Vienna *ab-initio* simulation package (VASP). Exchange and correlation effects were incorporated within the generalized gradient approximation (GGA), using the Perdew-Wang 91 (PW91) functional²⁷. Vosko-Wilk-Nusair interpolation²⁸ was used for the correlation part of the exchange correlation functional. Interaction between ions and electrons was described using the projector augmented wave method²⁹. Cutoff energy was set at 400 eV for the plane-wave basis. In all calculations, self-consistency was achieved with accuracy of at least 10^{-3} and 10^{-4} eV for the ionic and electronic loops respectively. All *k* points were generated using Γ -centered grids based on the Monkhorst-Pack scheme³⁰. The geometry of each periodic supercell has been optimized based on the perfect supercell.

For computational convenience, the primitive ZnO unit cell was redefined such that for the new basic unit, the *a*-axis now lies in the original [110]-direction while the *b*-axis lies in the original [110]-direction. This new basic unit has an orthorhombic crystal lattice that is twice the volume of the primitive hexagonal crystal lattice. The positions of the ions in the crystal are not changed. The pseudoferroelectric domain walls were modeled using a supercell consisting of two identical 180° (110) domain walls. The two 180° (110) domain walls were separated by 11 bilayers (31.3 Å). The model was a 62.6 Å × 33 Å × 5.3 Å supercell and the *k* points were generated with a 1 × 8 × 5 grid. Initial atomic structure at the boundary was modelled after Refs^{31,32}, based on what was termed as IDB* (Figs. 4e, 4f). IDB* can be structurally described as a simple IDB (see Supplementary Information, Fig. S9f) that has its inversion domain translated half a unit cell away from the [001]-direction. The twin grain boundary, on the other hand, was modeled using a supercell consisting of two identical twin (110) grain boundary. The two (110) twin boundaries are separated by 6 layers of ZnO (10.1 Å). This model was a 20.2 Å × 3.2 Å × 15.9 Å supercell and the *k* points that were generated with a 1 × 8 × 2 grid. The formation energy of two-dimensional (2D) defects was calculated by using: $E_f = \frac{1}{2}(E - E_{\text{bulk}})/A$, where *E* is the total energy of the supercell containing two such defects, E_{bulk} the total energy of the corresponding perfect supercell with no defects and *A* is the cross-sectional area of the defect. Bulk ZnO with and without V_{O} was modeled using supercells consisting of 3 × 3 × 2 unit cells, and *k* points were generated with a 3 × 3 × 2 grid.

In our calculation, the formation energy of a point defect *i* in neutral state was calculated by using: $E_f = E_{\text{tot}}^i - E_{\text{tot}}^0 + \sum_j n_j \mu_j$, where E_{tot}^i is the total energy of the supercell with defects, E_{tot}^0 the total energy of the corresponding perfect supercell, *n_j* the number of atoms removed, and μ_j the chemical potential of the corresponding atom. The actual chemical potential μ_i depends on experimental growth conditions

and ranges from Zn-rich conditions to O-rich conditions. In extreme O-rich condition, μ_{O} is given by the energy of O in an O₂ molecule while in extreme Zn-rich condition, μ_{Zn} is given by the energy of Zn in bulk hcp zinc. In this study, μ_{O} in O-rich condition was used as the reference and was set as the upper bound of μ_{O} at 0 eV. In addition, for Zn and O particle reservoirs to be at thermodynamic equilibrium with bulk ZnO, the following condition has to be satisfied as well: $\mu_{\text{Zn}} + \mu_{\text{O}} = E_{\text{ZnO}}$, where E_{ZnO} is the energy of ZnO. This set the lower bound of μ_{O} to be at -3.04 eV, which is the heat of formation of ZnO. Our calculated lattice parameters agreed very well with experimental results. For pure ZnO, the computed lattice parameters of $a = b = 3.29 \text{ \AA}$, $c = 5.29 \text{ \AA}$.

- Waser, R. & Aono, M. Nanoionics-based resistive switching memories. *Nat Mater* **6**, 833–840 (2007).
- Scott, J. F. & Araujo, C. A. P. D. Ferroelectric Memories. *Science* **246**, 1400–1405 (1989).
- Lee, S., Kim, H., Yun, D.-J., Rhee, S.-W. & Yong, K. Resistive switching characteristics of ZnO thin film grown on stainless steel for flexible nonvolatile memory devices. *Appl. Phys. Lett.* **95**, 262113 (2009).
- Yang, Y. *et al.* Observation of conducting filament growth in nanoscale resistive memories. *Nat Commun* **3**, 732 (2012).
- Joonhyuk, C. *et al.* Bipolar resistance switching characteristics in a thin Ti-Ni-O compound film. *Nanotechnology* **20**, 175704 (2009).
- Driscoll, T., Kim, H.-T., Chae, B.-G., Venra, M. D. & Basov, D. N. Phase-transition driven memristive system. *Appl. Phys. Lett.* **95**, 043503 (2009).
- Pershin, Y. V. & Di Ventra, M. Spin memristive systems: Spin memory effects in semiconductor spintronics. *Phys. Rev. B* **78**, 113309 (2008).
- Dal Corso, A., Posternak, M., Resta, R. & Baldereschi, A. Ab initio study of piezoelectricity and spontaneous polarization in ZnO. *Phys. Rev. B* **50**, 10715 (1994).
- Posternak, M., Baldereschi, A., Catellani, A. & Resta, R. Ab initio study of the spontaneous polarization of pyroelectric BeO. *Phys. Rev. Lett.* **64**, 1777–1780 (1990).
- Rodriguez, B. J., Gruverman, A., Kingon, A. I., Nemanich, R. J. & Ambacher, O. Piezoresponse force microscopy for polarity imaging of GaN. *Appl. Phys. Lett.* **80**, 4166–4168 (2002).
- Herng, T. S. *et al.* Mutual Ferromagnetic–Ferroelectric Coupling in Multiferroic Copper-Doped ZnO. *Adv. Mater.* **23**, 1635–1640 (2011).
- Wang, X. S., Wu, Z. C., Webb, J. F. & Liu, Z. G. Ferroelectric and dielectric properties of Li-doped ZnO thin films prepared by pulsed laser deposition. *Appl. Phys. A* **77**, 561–565 (2003).
- Yang, Y. C. *et al.* V⁵⁺ ionic displacement induced ferroelectric behavior in V-doped ZnO films. *Appl. Phys. Lett.* **90**, 242903–242901 (2007).
- Tagantsev, A. K. Pseudoferroelectricity: A possible scenario for doped ZnO. *Appl. Phys. Lett.* **93**, 202905–202903 (2008).
- Park, J. S. *et al.* Effects of interfacial layer structures on crystal structural properties of ZnO films. *J. Vac. Sci. Technol. A* **26**, 90–96 (2008).
- Shi, L., Shang, D. S., Sun, J. R. & Shen, B. G. Bipolar Resistance Switching in Fully Transparent ZnO:Mg-Based Devices. *Appl. Phys. Express* **2**, 101602 (2009).
- Ozgur, U. *et al.* A comprehensive review of ZnO materials and devices. *J. Appl. Phys.* **98**, 041301–041103 (2005).
- Shi, L. *et al.* Improved resistance switching in ZnO-based devices decorated with Ag nanoparticles. *J. Phys. D: Appl. Phys.* **44**, 455305 (2011).
- Tyrbell, T., Ahn, C. H. & Triscone, J.-M. Ferroelectricity in thin perovskite films. *Appl. Phys. Lett.* **75**, 856–858 (1999).
- Jesse, S., Lee, H. N. & Kalinin, S. V. Quantitative mapping of switching behavior in piezoresponse force microscopy. *Rev. Sci. Instrum.* **77**, 073702 (2006).
- Sounart, T. L. *et al.* Sequential nucleation and growth of complex nanostructured films. *Adv. Funct. Mater.* **16**, 335–344 (2006).
- Sato, Y., Yamamoto, T. & Ikuhara, Y. Atomic Structures and Electrical Properties of ZnO Grain Boundaries. *J. Am. Ceram. Soc.* **90**, 337–357 (2007).
- Callister, W. D. & Rethwisch, D. G. *Materials Science and Engineering* (Wiley, 2010).
- Chikazumi, S. & Charap, S. H. *Physics of Magnetism* (Krieger Publishing Company, 1978).
- Seidel, J. *et al.* Conduction at domain walls in oxide multiferroics. *Nat. Mater.* **8**, 229–234 (2009).
- Eliseev, E. A., Morozovska, A. N., Svechnikov, G. S., Gopalan, V. & Shur, V. Y. Static conductivity of charged domain walls in uniaxial ferroelectric semiconductors. *Phys. Rev. B* **83**, 235313 (2011).
- Wang, Y. & Perdew, J. P. Correlation hole of the spin-polarized electron gas, with exact small-wave-vector and high-density scaling. *Phys. Rev. B* **44**, 13298 (1991).
- Vosko, S. H., Wilk, L. & Nusair, M. Accurate spin-dependent electron liquid correlation energies for local spin density calculations: a critical analysis. *Can. J. Phys.* **58**, 1200–1211 (1980).
- Kresse, G. & Joubert, D. From ultrasoft pseudopotentials to the projector augmented-wave method. *Phys. Rev. B* **59**, 1758 (1999).
- Monkhorst, H. J. & Pack, J. D. Special points for Brillouin-zone integrations. *Phys. Rev. B* **13**, 5188 (1976).



31. Northrup, J. E., Neugebauer, J. & Romano, L. T. Inversion domain and stacking mismatch boundaries in GaN. *Phys. Rev. Lett.* **77**, 103–106, doi:10.1103/PhysRevLett.77.103 (1996).
32. Yan, Y. F. & Al-Jassim, M. M. Inversion domain boundaries in ZnO: First-principles total-energy calculations. *Phys. Rev. B* **69**, 085204 (2004).

Acknowledgements

The work is supported by NRF-CRP R284–000-056–281 and MoE AcRF R265-000-406-112.

Author contributions

J.D. and K.Y.Z conceived and designed the experimental and theoretical work. T.S.H. fabricated the ZnO films and performed XRD, Hall Effect analysis, TEM, SEM, EDS, PL, XPS and Raman studies. A.K. carried out the C-AFM, resistance switching, PFM and PFS measurement and A.K performed the corresponding results analysis. C.S.O. developed the

model and performed 1st principle calculation. Y.P.F. provided technical guide in modeling/simulation. T.S.H and C.S.O drafted the manuscript which has been further revised by all authors. T.S.H. and A.K. contributed equally in this work.

Additional information

Supplementary information accompanies this paper at <http://www.nature.com/scientificreports>

Competing financial interests: The authors declare no competing financial interests.

License: This work is licensed under a Creative Commons Attribution-NonCommercial-NoDerivative Works 3.0 Unported License. To view a copy of this license, visit <http://creativecommons.org/licenses/by-nc-nd/3.0/>

How to cite this article: Herng, T.S. *et al.* Investigation of the non-volatile resistance change in noncentrosymmetric compounds. *Sci. Rep.* **2**, 587; DOI:10.1038/srep00587 (2012).